Measurements of the Photon Structure Function at L3

F.C. Erné[a]

[a]NIKHEF, P.O. Box 41882, 1009 DB Amsterdam, The Netherlands

New measurements of the photon structure function in the Q^2 ranges between 1 and 9 GeV^2, 9 and 30 GeV^2 and between 40 and 500 GeV^2 are presented. The data have been taken by L3 with the LEP e^+e^- collider at the center-of-mass energies of 91 and 183 GeV with integrated luminosities of 140 and 52 pb^{-1}.

1. Introduction

Deep-inelastic electron scattering on a photon target provides interesting tests of quantum chromodynamics (QCD). The photon structure function F_2^γ is derived from measurements on the reaction $e^+e^- \rightarrow e^+e^- +$ hadrons tagged by the detection of one of the final-state electrons. In most collisions the other electron scatters at such a small angle that it remains undetected, leading to a single-tag measurement. The virtual photons associated with momentum transfers Q^2 and P^2 are referred to as "probe" and "target" photons respectively, with $Q^2 >> P^2$. The structure function is expressed as a function of $x = Q^2/(P^2+Q^2+W_{\gamma\gamma}^2)$, Q^2 and P^2, where $W_{\gamma\gamma}$ is the invariant mass of the produced hadrons and x the Björken scaling variable.

F_2^γ receives contributions from direct quark-antiquark production which can be calculated in perturbative QCD, a vector dominance term which describes non-perturbative transitions from photons to vector mesons and their subsequent hadronic interactions, and resolved photon processes in which one of the photons emits a hadronic jet and a gluon that collides with a direct of resolved photon. At high x the quark constituents of the photon are dominant, at low x the gluon constituents. F_2^γ is not predictable where VDM and resolved photons become important. Parameterizations employ an ansatz for F_2^γ at a certain value $Q^2 = Q_0^2$, and a QCD evolution to the Q^2 value of the data. Comparisons will be shown with GRV-LO/HO[1], SaS[2], LAC[3], AGF[4] and LRSN[5] parameterizations.

Table 1
Data samples

$\sqrt{s}$	θ_{tag}	Q^2	P^2	events
GeV	mrad	GeV^2	GeV^2	
91	26-66	1.2-9	0.08	9928
183	30-66	9-30	0.08	1694
91	200-600	40-500	0.014	496
91	200-600	40-500	1-8	43

2. Data analysis

Some characteristics of the data samples are shown in Table 1. The low- and medium Q^2 single-tag data have been published recently[6], [7], while the high-Q^2 data are preliminary.

The analyses use cuts on the electron-tag energy, the visible mass, the summed transverse momentum, antitag definition and the number of charged-particle tracks. The high-Q^2 analysis uses additional cuts on event rapidity and thrust direction in the $\gamma\gamma$ center-of-mass momentum.

Several Monte Carlo calculations have been employed to calculate the L3 acceptance and as input for resolution calculations. In JAMVG[8] the Quark Parton Model is implemented with light-quark masses of 0.325 GeV and a charm-quark mass of 1.6 GeV, in PHOJET[9] $\gamma\gamma$ processes are described within the Dual Parton Model in terms of Reggeon and Pomeron exchanges, while TWOGAM[10] generates three different $\gamma\gamma$ processes separately, the QPM, soft hadronic VDM processes and the QCD resolved photon contribution.

2.1. $W_{\gamma\gamma}$ measurement

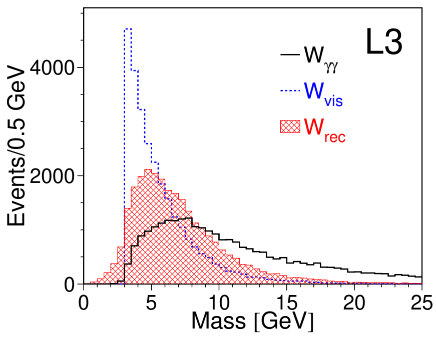

Figure 1. Monte Carlo (PHOJET) comparison of the distribution of the generated two-photon mass, $W_{\gamma\gamma}$, with those of W_{vis}, the mass reconstructed with the measured particles, and W_{rec}, the mass obtained by employing tag kinematics and transverse momentum conservation.

The hadronic final state is reconstructed from tracks and calorimetric clusters, but not completely due to detector acceptance. Therefore the visible mass W_{vis} is generally smaller that $W_{\gamma\gamma}$, and x_{vis} larger than x. In the L3 collaboration two ideas were explored to improve the $W_{\gamma\gamma}$ measurement.

The first method[11] exploits transverse momentum conservation and approximates the term $(E+p_z)$ in equation (1) in a way similar to the Jaquet-Blondel method in electron-proton scattering.

$$W_{vis}^2 = (E+p_z)(E-p_z) - p_t^2 \tag{1}$$

with $E = \sum_i E^i$, $p_z = \sum_i p_z^i$ and $p_t = |\sum_i \vec{p}_t^i|$ and the sum over the hadronic energy vectors, is replaced by

$$W_{rec}^2 = (2E^{beam} - E^{tag} - p_z^{tag})(E-p_z) - (p_t^{tag})^2 . \tag{2}$$

As is shown in Fig. 1, W_{rec} improves on the W_{vis} measurement at low mass. The method, combined with Baysian unfolding, has been employed in the low- and medium Q^2 measurements.

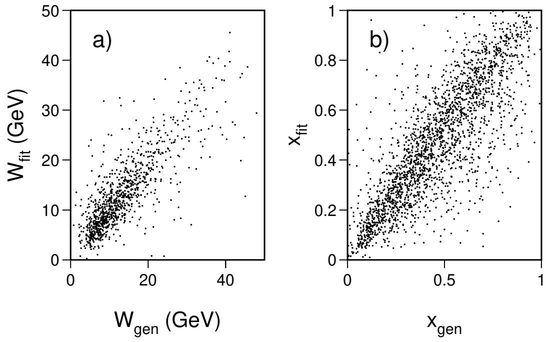

Figure 2. Correlations between the values generated by the JAMVG Monte Carlo and those obtained after the kinematic fit for a) $W_{\gamma\gamma}$ and b) x.

In the high-Q^2 analysis the resolution is improved by kinematic fitting. The following expression is minimized:

$$\begin{aligned}
\chi^2 &\equiv \sum_{i,j} V_{i,j}^{-1} \Delta p_i \Delta p_j + \sum_k W_k C_k^2, && (3)\\
\Delta p_1 &\equiv E - \sum_l E_l^h, && (4)\\
\Delta p_2 &\equiv p_z - \sum_l p_{z,l}^h, && (5)\\
\Delta p_3 &\equiv p_{in} - \sum_l p_{in,l}^h . && (6)
\end{aligned}$$

Here, $(E, \vec{p})$ is the four-momentum of the hadronic system; p_{in} is its transverse momentum in the scattering plane. $(E^{\pm}, \vec{p}^{\pm})$ are the electron four-momentum vectors. The constraints are:

$$\begin{aligned}
C_1 &= E^- + E^+ + E - 2E_{beam} + 2RC = 0, && (7)\\
C_2 &= p_z^- + p_z^+ + p_z = 0, && (8)\\
C_3 &= p_{in}^- + p_{in}^+ + p_{in} = 0. && (9)
\end{aligned}$$

The error matrix V and the weight factors W depend on measurement errors on hadrons and electrons, respectively. The term RC is an estimate of the average radiative correction to be applied for Monte Carlo data. It is set to zero for real data. For single-tag data one combines C_1, C_2: $E^+ = -p_z^+$ and $p_{in}^+ = 0$. The mean values of

$C_1 - C_3$ are adjusted to zero by an overall scale factor for the hadronic energy. The fit allows a calculation of

$$W_{fit}^2 = E^2 - p_{in}^2 - p_{out}^2 - p_z^2 \quad (10)$$

as well as the momentum of the target photon. A transformation to the $\gamma\gamma$ center-of-mass system can be made after the fit. As is shown in Fig. 2, the relations between the generated and fitted two-photon masses and x values are on average linear for the events generated with JAMVG. Similar correlations can be found with the other generators PHOJET and TWOGAM, though with less good resolution. Unfolding is achieved by the SVD program[12].

3. Results on the low and medium Q^2 data

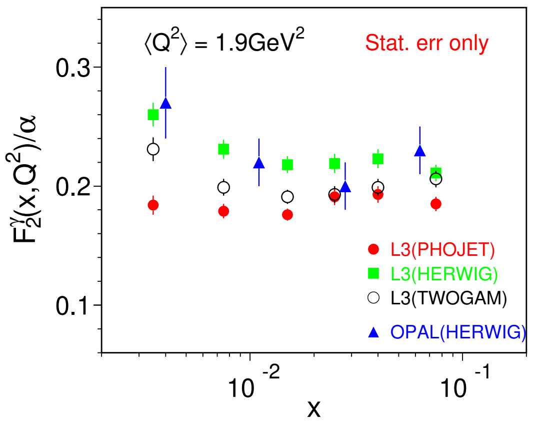

Figure 3. The measured F_2^γ/α at $< Q^2 >= 1.9$ GeV^2 after unfolding with three different Monte Carlo models.

As is shown in Fig. 3 the Baysian unfolding procedure, which derives x from x_{rec}, yields results which are approximately independent of x down to $x = 5 \times 10^{-3}$ at $< Q^2 >= 1.9$ GeV^2. However they do depend on the Monte Carlo model at the 10-30% level. There is good agreement with results from the OPAL experiment[13] if the same model is used. The values of F_2^γ/α in two different Q^2 bins after unfolding with PHOJET are shown in Fig. 4. One observes that the GRV-HO[1] predictions give a good description of the data at low x, while LAC1[3] agrees with the data at $Q^2 = 5$ GeV^2. The SaS-1d[2] predictions lie below the data. The effect that $< P^2 >= 0.08$ GeV^2 would decrease the SaS-1d prediction by about 15%.

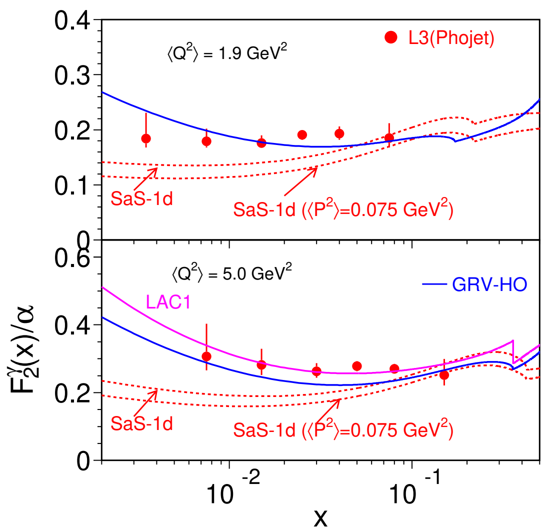

Figure 4. The measured F_2^γ/α at $< Q^2 >= 1.9$ GeV^2 and $< Q^2 >= 5.0$ GeV^2. The data are compared with the predictions of GRV-HO, SaS-1d, LAC1 at $P^2 = 0$, and SaS-1d at $P^2 = 0.075$ GeV^2. The change of shape of predictions at large x is due to the charm threshold.

In Fig. 5 the values for F_2^γ/α in three different intervals at medium Q^2 are compared with model predictions. At values of x larger than 0.1 there is good agreement with GRV-HO[1], SaS-1d[2] and LAC1[3]. Below x=0.1 the data lie between LAC1 and GRV-HO.

4. Results on the high Q^2 data

In Fig.6 kinematic distributions in the $\gamma\gamma$ center of mass of the selected single-tag events are compared with Monte Carlo distributions. In 6a) the distribution of the cosine of the thrust polar

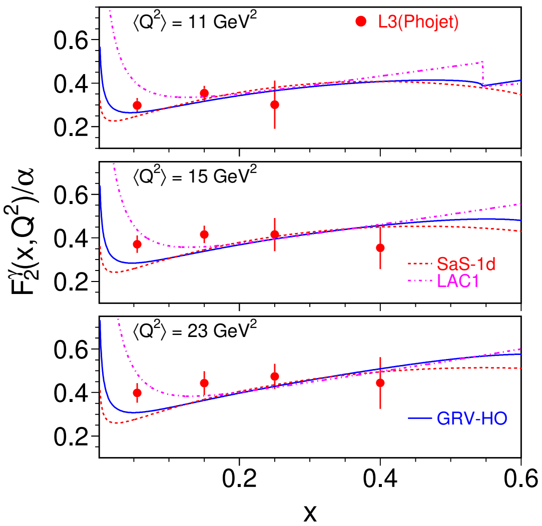

Figure 5. The measured F_2^γ/α at $< Q^2 >= 10.8$ GeV^2, $< Q^2 >= 15.3$ GeV^2 and $< Q^2 >= 23.1$ GeV^2 after unfolding with PHOJET. The statistical and systematic errors are added in quadrature. The data are compared with the predictions of GRV-HO, SaS-1d and LAC1.

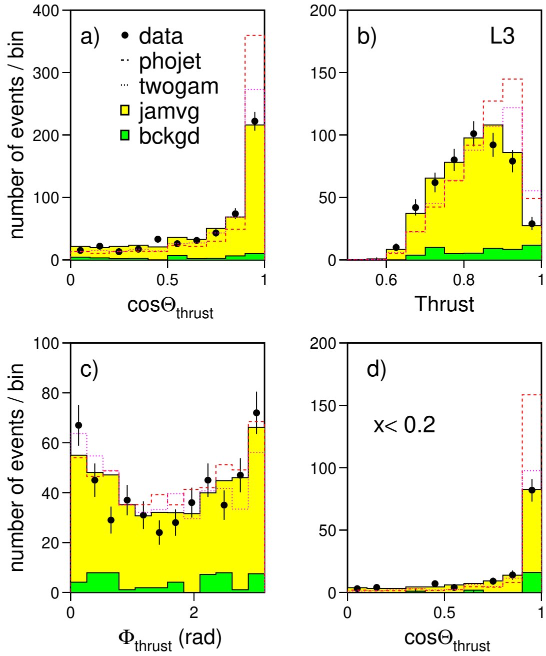

Figure 6. The distribution of a) $\cos\theta(thrust)$, b) the thrust, c) $\phi(thrust)$ and d)$\cos\theta(thrust)$ for events with $x_{fit} < 0.2$ in the $\gamma\gamma$ center-of-mass frame for single-tag events in bins of 0.1, 0.05, $\pi/10$ and 0.1 respectively. The JAMVG (shaded histogram), PHOJET (dashed histogram) and TWOGAM (dotted histogram) contributions are scaled to have the same number of events in data-background and MC.

angle with respect to the $\gamma\gamma$ axis shows forward peaking in good agreement with the JAMVG simulation. The data show no indication for the diffractive forward peak in PHOJET and in TWOGAM. The same is true for the low-x selection shown in 6d). In 6b) the thrust exhibits a wide distribution in the data, which is adequately described by the color-connected fragmentation in JAMVG and less well by the fragmentation strategies in PHOJET and TWOGAM. The ϕ distribution shows an accumulation in the scattering plane, while the generated distribution is approximately flat; this distortion is due to the incomplete kinematic constraints in the single-tag events. Fig. 7 shows the physics distributions for a) x_{fit}, b) y_{fit}, c) Q^2 and d) W_{fit} in the selected single-tag events. The x_{fit} distribution is limited by the maximum mass observed, $W_{fit} \approx 40$ GeV, and by the minimum mass of $W_{fit} = 3$ GeV and because Q^2 lies between 40 and 500 GeV^2. There is an excess of events over the QPM prediction at $x_{fit} < 0.3$ and $y_{fit} > 0.3$, which clearly shows the importance of a QCD contribution in the measured Q^2 range. The Q^2 distribution follows the QPM shape; the hadronic mass has an excess over the QPM at masses above 20 GeV. In Fig. 8a) the structure function F_2^γ/α for real photons at $< Q^2 >= 120$ GeV^2 is compared with the QPM calculation[14], and with the QCD calculations GRV-HO[1], SaS-1d[2], AGF[4] and LRSN[5]. The measurements show a low-x excess over these calculations. In Fig. 8b) the effective structure function F_{eff}^γ/α for virtual photons at $< Q^2 >= 120$ GeV^2 and $< P^2 >= 3.7$ GeV^2 is compared with the QPM calculation and with

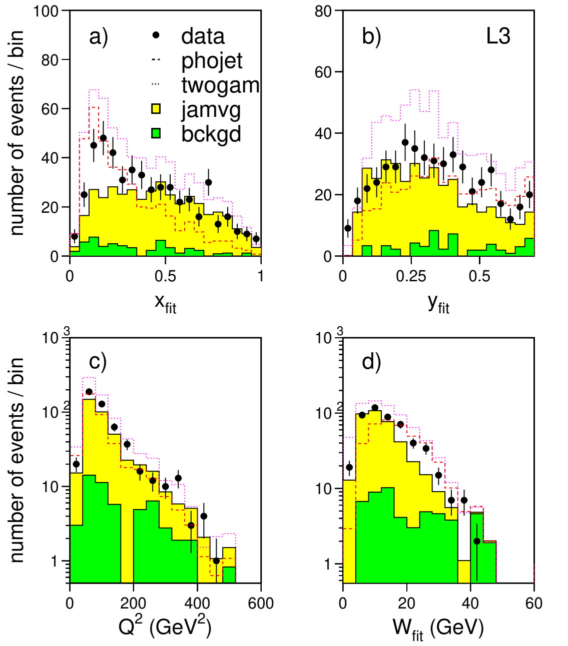

Figure 7. The a) x_{fit}, b) y_{fit}, c) Q^2 and d) W_{fit} distributions for single-tag events in bins of 0.05, 0.035, 40 GeV^2 and 5 GeV, respectively. The data are compared with JAMVG (shaded histogram), PHOJET (dashed histogram) and TWOGAM (dotted histogram) predictions. The MC distributions are normalized to the integrated luminosity of the data.

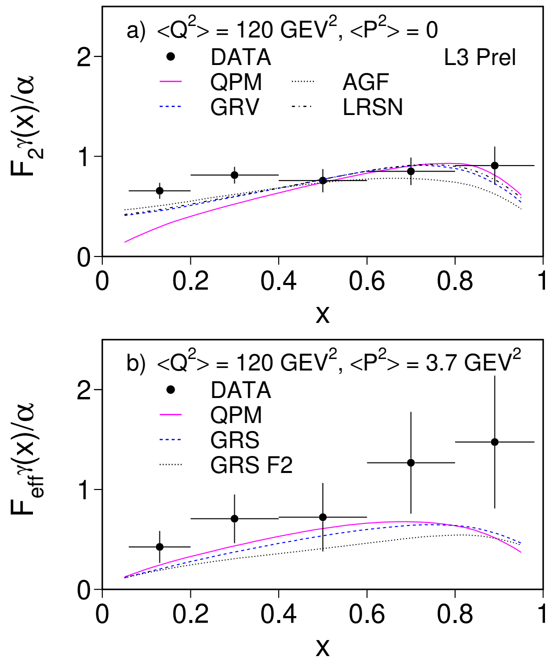

Figure 8. The structure function F_2^γ/α for real photons at $< Q^2 >= 120$ GeV^2, and b) F_{eff}^γ/α for virtual photons at $< Q^2 >= 120$ GeV^2 and $< P^2 >= 3.7$ GeV^2, compared with calculations described in the text.

a QCD calculation for virtual photons[15]. The QCD calculation pertains to F_2^γ/α only, which is indicated by 'GRS F2'. To compare with the data, we added the contributions from longitudinal target photons estimated from the QPM to these structure functions. This is indicated by 'GRS'. The measurements are compatible with the calculations, apart from a difference in normalization.

5. Evolution with Q^2 and P^2

In Fig. 9a) the structure function F_2^γ/α for real photons versus Q^2 for the x-ranges 0.01-0.1, 0.1-0.2 and 0.2-0.3 is compared with GRV-LO, SaS-1d and LAC1 parameterizations. In Fig. 9b) the structure function F_2^γ/α for the x-range 0.05-0.98 compared with the QPM calculation based on ref.[14] and the QCD calculation by Laenen et al.[5]. For virtual photons quark distribution functions approximately depend on $\ln(Q^2/P^2)$; for the L3 data and earlier PLUTO[16] data this quantity is approximately equal to 3. In Fig. 10a) the measurements on F_{eff}^γ/α in the x range 0.05-0.75 are compared with the QPM calculation based on ref.[14] versus Q^2 for $\ln(Q^2/P^2)$=3. In Fig. 10 b) the structure function F_{eff}^γ/α for virtual photons versus P^2 for the x-range 0.05-0.98 is compared with the same QPM calculation. The agreement with the predicted evolutions in Q^2 and P^2 is satisfactory.

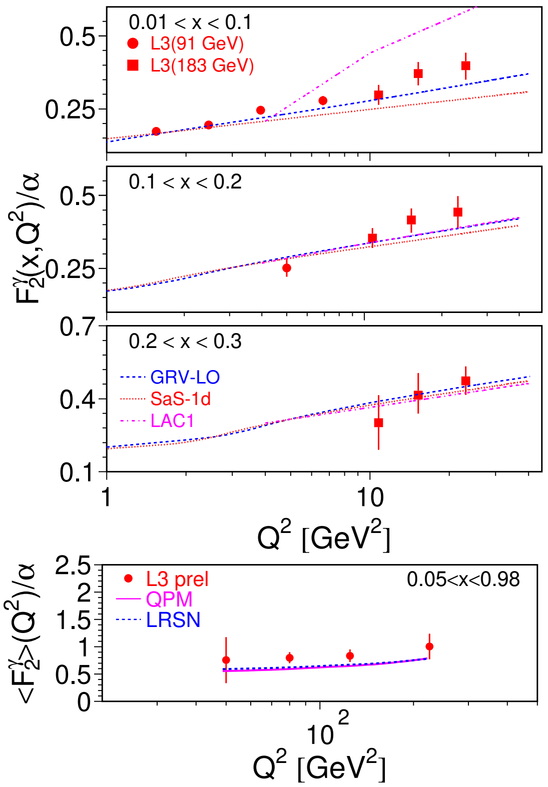

Figure 9. a) The measured F_2^γ/α for real photons versus Q^2 for the x-ranges 0.01-0.1, 0.1-0.2 and 0.2-0.3. b) The measured F_2^γ/α for real photons versus Q^2, for the x-range 0.05-0.98, compared with calculations mentioned in the text.

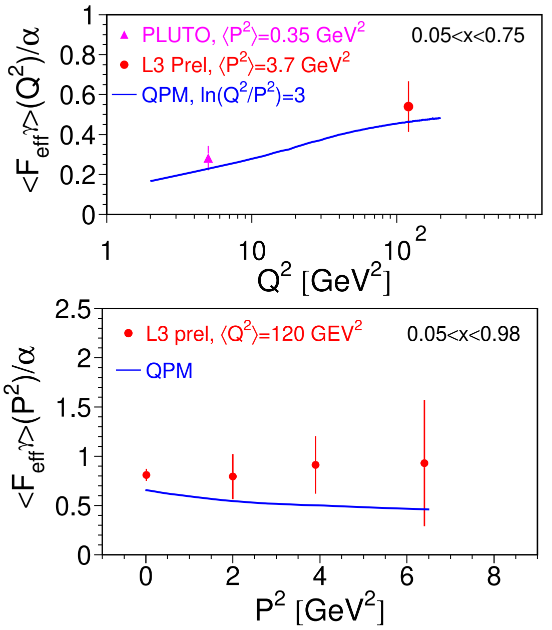

Figure 10. a) The measured F_{eff}^γ/α for virtual photons versus Q^2 for the x-range 0.05-0.75 compared with data form PLUTO and the QPM calculation described in the text for $\ln(Q^2/P^2) = 3$. b) The measured F_{eff}^γ/α for virtual photons versus P^2 for the x-range 0.05-0.98 compared with the QPM calculation described in the text.

REFERENCES

1. M. Glück, E. Reya and A. Vogt, Phys. Rev. D 45 (1992) 3986; Phys. Rev. D 46 (1992) 1973.
2. G.A. Schuler and T. Sjöstrand, Z. Phys. C 68 (1995) 607; Phys. Lett. B376 (1996) 193.
3. H. Abramovicz, K. Charcula and A. Levy, Phys. Lett. B269 (1991) 458.
4. P. Aurenche, J.-P. Guillet and M. Fontannaz, Z. Phyz. C64 (1994) 621.
5. E. Laenen, S. Riemersma, J. Smith and W.L. van Neerven, Phys. Rev. D49 (1994) 5753; E. Laenen and S. Riemersma, Phys. Lett. B376 (1996) 169.
6. L3 collab., Phys. Lett. B436 (1998) 403.
7. L3 collab., Phys. Lett. B447 (1999) 147.
8. J.A.M. Vermaseren, Nucl. Phys. B229 (1983) 347.
9. R. Engel, Z. Phyz. C66 (1995) 203; R. Engel and J. Ranft, Phys. Rev. D54 (1996) 4244.
10. S. Nova and T. Todorov, DELPHI Note 90-35 (1990).
11. Physics at LEP2, CERN 96-01, Vol. 2, 201.
12. A. Hoecker and V. Kartvelishvili, NIM A372 (1996) 469.
13. OPAL collab., Phys. Lett. B412 (1997) 225.
14. V.M. Budnev et al, Phys. Rep. 15C (1975) 181.
15. M. Glück, E. Reya and M. Stratmann, Phys. Rev. D 54 (1996) 5515.
16. PLUTO collab., Phys. Lett. 142 (1984) 119.